DOI: 10.4408/IJEGE.2011-03.B-035

EXPERIMENT ON THE STABILITY OF GRANULAR SOIL SLOPES BY RAINFALL INFILTRATION

Rong-Her CHEN(*), Kwo Jane KUO(**) & Chih-Ming CHANG(***)

(*) Professor, Department of Civil Engineering, National Taiwan University, Email: rongherchen@ntu.edu.tw, 886-2-23629851
(**) PhD student at National Taiwan University, E-mail:clay.kuo@msa.hinet.net
(**) Former master's student at National Taiwan University

ABSTRACT

Slope failure is commonly caused by rainfall infiltration due to increase in pore-water pressure within the slope. In order to understand the failure mechanism of granular soil slopes, a model slope subjected to rainfall infiltration was developed and employed to perform experiment on sandy soils. Different geological conditions, fines contents of sand, and rainfall intensities were considered as variables. Infiltration of rainfall was simulated by an overland flow infiltrating uniformly into a platform on the top of the slope. During the experiment, the variations in pore water pressure and volumetric water content in the soil were measured. The characteristics of the failure mechanism and the responses of pore pressure and water content in four model slopes were observed and discussed. According to the observation, the failure in permeable sand was a sliding mode. Initial failure was noticed as a piping occurred at the toe of slope, and it then gradually propagated upward as a retrogressive failure. However, the failure in less permeable silty sand was initiated by erosion at shallow depth, the rill later expanded and turned into either a flow or a complex mode of flow and slide, depending on the rainfall intensity applied. Moreover, sandy soil had a marked increase in pore-water pressure when approaching failure; but this phenomenon was less obvious in silty sand.

***Key words**: model test, slope, stability, granular soil, infiltration*

INTRODUCTION

Many slope failures were caused by infiltration of water that induced increase in pore-water pressure and seepage force in soil (Lump, 1975; Brand, 1982; Iverson & Major, 1986; Chen *et alii*, 1999; Kim *et alii*, 2004; Chen *et alii,* 2004; Chen *et alii*, 2009). The stability of an unsaturated soil slope can be dramatically altered as the soil becomes gradually saturated, even resulting in a slope failure. The collapsed soil may turn into a flow if there is plenty of water in the soil along with favourable geological condition.

Using model tests to study rainfall induced slope failures have been conducted by a few research. Wang & Sassa (2003) performed tests on silica sand of different initial dry densities and fines contents to investigate the effects of grain size on pore-water pressure generation and the failure behaviour of rainfall-induced landslides. Moriwaki *et alii* (2004) conducted a full-scale experiment to clarify the failure process of landslide triggered by rainfall. The soil was loose sand with a relative density of 35 % and an initial water content of 8 %. The flume was subjected to rainfall of an intensity of 100 mm/hr. The sliding process of the slope was recorded and evaluated by measuring the displacement of slope surface, and the piezometric level and pore-water pressure within the soil. Orense *et alii* (2004) conducted model sandy slopes to investigate slope failure by water percolation from side upslope, with a 80 cm constant height, and by artificial rain falling on the slope with rainfall intensities

of 42~262 mm/hr. The material was silty sand with 9% of fines content. The soil samples were obtained from Omigawa landslide site in Japan. The maximum rainfall intensity was 42 mm/hr in that area.

A set of laboratory-scale experiment for studying rainfall induced slope failure was performed by Tohari *et alii* (2007). The soils were sand and residual granite soil of various relative densities and initial water contents. They employed two types of water supply in the study; one was a rainfall simulator designed to produce an effective rainfall intensity of approximately 100 mm/hr, and the other was a water tank which could vary the rising rate of water level within the slope. Huang *et alii* (2008) also conducted model tests on sandy soil slopes to look into the rainfall-induced failure process in the slope. In addition, they observed and reported the characteristics of cumulative solid discharge versus time.

Chen *et alii* (2004) investigated the triggering mechanism for a hazardous mudflow caused by a typhoon which delivered approximately 300 mm/day of precipitation. The destructive 50-m long mudflow rushed down a hill without any forewarning from a man-made platform of 30 m x 80 m right at the top of the mudflow. This funnel-shaped mudflow of a volume of 2,000 m^3 damaged three houses below and resulted in five deaths. According to the test results of the samples taken from the erosion gully, most of soils belong to silty and clayey sand. The bedding, which appears in the erosion gully, has a dip angle ranging from 30° to 60° toward the toe of the slope. Besides, the cause of the disaster was found likely due to the malfunction of the drainage system around the platform because more overland flow on the platform could infiltrate into the slope. This disaster was deeply concerned for the disaster area occurred in an urbanized territory.

For a better understanding about relevant slopes as the case study described above, model test was employed to study the failure mechanism of soil slopes composed of sand and silty sand, respectively. Different geological conditions, fines contents of sand and rainfall intensities were considered as variables to test the stabilities of model slopes. The infiltration of rainfall was simulated by an overland flow infiltrating uniformly from the top of the slope. The characteristics of the failure mechanism and the responses of pore pressure and water content for four model slopes were observed and are discussed below.

Physical quantity	Relationship
Length	$L_m = (1/\lambda)\, L_p$
Slope angle	$\theta_m = \theta_p$
Unit weight	$\gamma_m = (1/\rho)\, \gamma_p = \gamma_p$
Friction angle	$\phi_m = \phi_p$
Pore-water pressure (or stress)	$u_m = (1/\alpha)\, u_p = (1/\lambda)\, u_p$
Strain	$\varepsilon_m = (1/\beta)\, \varepsilon_p = \varepsilon_p$
Time	$t_m = (1/\tau)\, t_p = (1/\sqrt{\lambda})\, t_p$
Rainfall intensity (or velocity)	$i_m = (\tau/\lambda)\, i_p = (1/\sqrt{\lambda})\, i_p$
Hydraulic conductivity	$k_m = (\tau/\lambda\beta)\, k_p = (1/\sqrt{\lambda})\, k_p$

Note that λ, ρ, α, β, and τ are the scaling factors for length, unit weight, stress, strain, and time, respectively. In this study, ρ and β are equal to 1.

Tab. 1 - Dimensional analysis of the physical quantities in model test

MODEL TEST

Two kinds of samples were tested; sample A was composed of 100% sand and sample B was a mixture of 90 % sand and 10 % silt. According to the Unified Soil Classification System, samples A and B are classified as SP and SM, respectively. Therefore, they are expected to behave differently under rainfall infiltration.

SIMILARITY ANALYSIS

In the studies on slope failure, model test is one of the efficient methods. This is because model test has the merits that it can be performed in well controlled conditions, e.g., boundary and loading conditions; more importantly, it can also simulate how a slope failure is initiated and also the whole process of failure can be observed in the laboratory.

In a model test, the model and the prototype should be related through satisfying the geometric similarity, the kinematic similarity, and the dynamic similarity so that the feasibility and reliability of test results are ensured. For instance, the scaling factor of length between the prototype and the model can be chosen as λ (= L_p/L_m) and the materials used in the prototype-slope and the model-slope can have the same unit weight. From similarity analysis (Rocha, 1957; Roscoe, 1968), the relationship between the physical quantities of prototype- and model- slopes are obtained as shown in Table 1.

EXPERIMENT SETUP

The experimental setup is shown in Figures 1a and 1b for different geological conditions. The device includes a sand tank supported by a steel frame; the

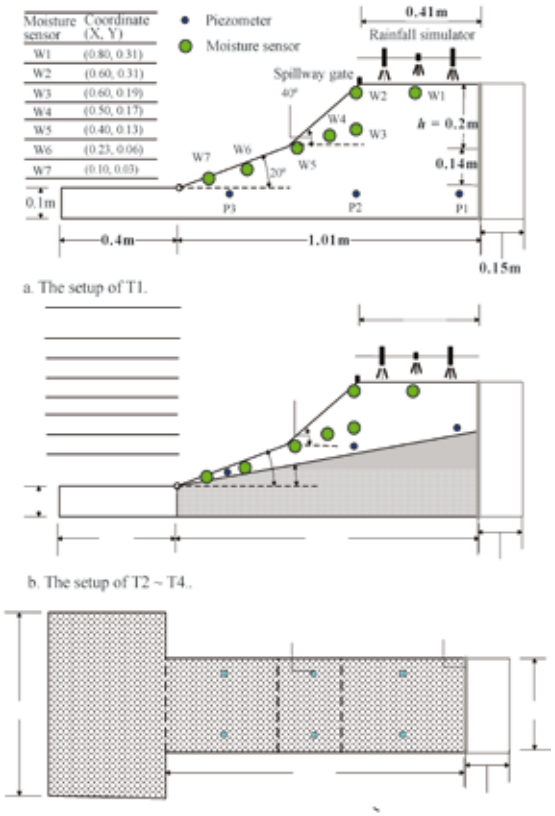

Fig. 1 - Experimental setup

wall of the device is made of 10-mm thick reinforced glass. The profile of the slope has two sections: a 40° upper slope and a 20° lower slope, with a platform at the top of the slope. This geometric configuration was arranged in order to study the failure mechanism of concave steep slopes. It is also hoped that the result from this experiment may provide a reference for future remedial work of similar slopes. The flow chute is 0.3 m wide, while that of the deposition area is 0.6 m wide and 0.4 m long (Figure 1c).

A rainfall device is set directly above the platform. Water can also be supplied from either the bottom or the rear of the tank to simulate the change of ground water level.

Several moisture sensors, Delta-T SM200, are used to measure the volumetric water content of the soil. The accuracy of the sensor is ±3 %, with an operating range between 0-60°. Moisture sensors W1~W7 are installed on one side of the tank as shown in Figures 1a and 1b. Pore-water pressures are recorded by piezometers, Kyowa PGM-G. The accuracy is ± 0.5 %, and the allowable pressure is 20 kPa. The piezometers are installed either as shown in Figure 1a for a homogeneous soil slope, or as shown in Figure 1b for a slope with an impervious dip stratum of 10° underneath.

Moreover, three CCD cameras are aimed at different angles, normal to the side of the tank, the lower slope and the deposition area, to record the process of the test. These cameras have a resolution of 640×480 pixels and the maximum frame rate is 30 fps.

TEST MATERIAL

The sand used for testing is uniform, sub-angular, and contains 99.8% silica. It is classified as poorly-graded sand (*SP*) as per the Unified Soil Classification System, with a coefficient of uniformity of C_u = 1.566, and a coefficient of curvature of C_c = 0.946. The physical properties of the sand are: maximum unit weight $\gamma_{d,max}$ = 16.9 kN/m^3, minimum unit weight $\gamma_{d,min}$ = 14.6 kN/m^3, median diameter d_{50} = 0.2 mm, and effective grain size d_{10} = 0.13 mm.

The friction angles of the sand are obtained by triaxial consolidated-undrained test at relative densities of 55 % and confining pressures of 50, 100, and 200 kPa, respectively. The friction angles of samples A and B are 36.6° and 35.1°, respectively. Furthermore, samples A and B have hydraulic conductivities of 3×10^{-4} m/s and 4×10^{-5} m/s, respectively. The saturated volumetric water content of soil is obtained from the soil-water characteristics curve using pressure plate test; the values are 41.9% and 47.1% for samples A and B, respectively.

TEST PROGRAM

The test program is shown in Table 2. The parameters considered include geological condition, silt content in sand, and rainfall intensity. Two geological conditions are the homogeneous slope (Figure 1a) and the slope with an impervious dip stratum (Figure 1b). The latter was to

Test	Sample	Silt content (%)	Geological condition	Rainfall intensity (mm/hr)
T1	A	0	homogeneous soil	286
T2	A	0	soil/dip stratum	286
T3	B	10	soil/dip stratum	286
T4	B	10	soil/dip stratum	140

Tab. 2 - Test program

research the effect of impervious dip stratum. In addition, due to relatively low hydraulic conductivity of sample B, only one homogeneous slope was studied for sandy soil.

The rainfall intensity chosen was based not only on the hydraulic conductivity of the soil, but also on the site. The higher value of rainfall intensity, 286 mm/hr or 8 $x10^{-5}$ m/s, was calculated from the empirical equation for Taipei City (Chen *et alii*, 2004); the lower value, 140 mm/hr or 3.8 $x10^{-5}$ m/s, was chosen to be equal to the hydraulic conductivity of sample B. Based on our previous studies, these values exceeded the threshold value of 80 mm/hr for slope failure to occur. Furthermore, because of the pervious nature of sample A, it was tested only under high rainfall intensity.

Strictly speaking, according to Table 1, the rainfall intensity and the hydraulic conductivity of the soil should be modified when conducting a model test. However, the hydraulic conductivity of the soil is so small that the modified value seems to have little effect on the test results. Moreover, the scaling factors for these two quantities are the same. Accordingly, the rainfall intensity was not modified either.

TEST PROCEDURE

The test procedures are briefly described as following.

1. For constructing the homogeneous slope, a layer of sand of 0.1 m thick was placed at the bottom of the tank at first. When constructing the non-homogeneous slope, a 10° stratum made of plywood was placed in the beginning. After that, the gap between this stratum and the wall of the tank was sealed with silicone sealant for waterproof.
2. The slope was formed with the help of a shaping plate to retain soil in place. The soil was then pluviated by layers to obtain a uniform sand deposit, each being 0.02 m thick, from the bottom to the top. The plate was lifted every time a layer of soil had been placed. This procedure was repeated till a specified full height was reached.
3. After the model slope had been constructed, a bar working as a spillway gate was placed at the fringe of the platform. This bar was 0.3 m long and 0.018m high. The purpose of using it was to retain surface water to simulate an overland flow.
4. The water valve at the bottom of the tank was opened to allow water to flow slowly into the tank at a rate of 0.01 m^3/min. After the water table had reached the top of the slope, the valve was closed. The slope was then left 24 hours for soaking in order to reach as much saturation as possible.
5. Then the valve was opened again to drain out water until the water table was lowered to the elevation at the toe of the slope. It usually took about two hours for water drainage, e.g., at a rate of 0.02 m^3/min, so that soil settlement was insignificant.
6. The monitoring system was turned on; it included three CCDs, pore-water pressure transducers and piezometers.
7. The infiltration test was started by turning on the rainfall device to generate rainfall at a specified intensity.
8. During the test, the volumetric water content and pore-water pressure were recorded at frequencies of 5/s and 1/s, respectively.
9. When there was no significant soil movement observed, the test was stopped.

Note that soaking soil before the test was not only to simulate the effect of precedent rainfall on site but also to expedite the test.

TEST RESULTS AND DISCUSSION

Before discussing test results, the definition of symbols for several important points during a test are given, i.e., t_p = the time to occur initial failure when piping was observed, t_f = the time when an obvious mass movement was initiated, and t_e = the time at the end of significant mass movement. The failure mode and important time points of each test are tabulated in Table 3.

FAILURE PROCESS

Based on the observation, the failure mode of sample A belongs to a sliding mode; a typical example is displayed in Figure 2 and the whole process is presented in Figure 3. However, sample B failed more like a flow. The reason could be attributed to their hydraulic conductivities and fines content. Sample A was composed mainly of relatively permeable sand and the seepage with high velocity could be expected

Test	Failure mode	t_p (s)	t_f (s)	t_e (s)
T1	Slide	30	120	240
T2	Slide	20	40	270
T3	Flow	40	130	370
T4	Slide/Flow	80	140	362

Tab. 3 - Important time points of each test

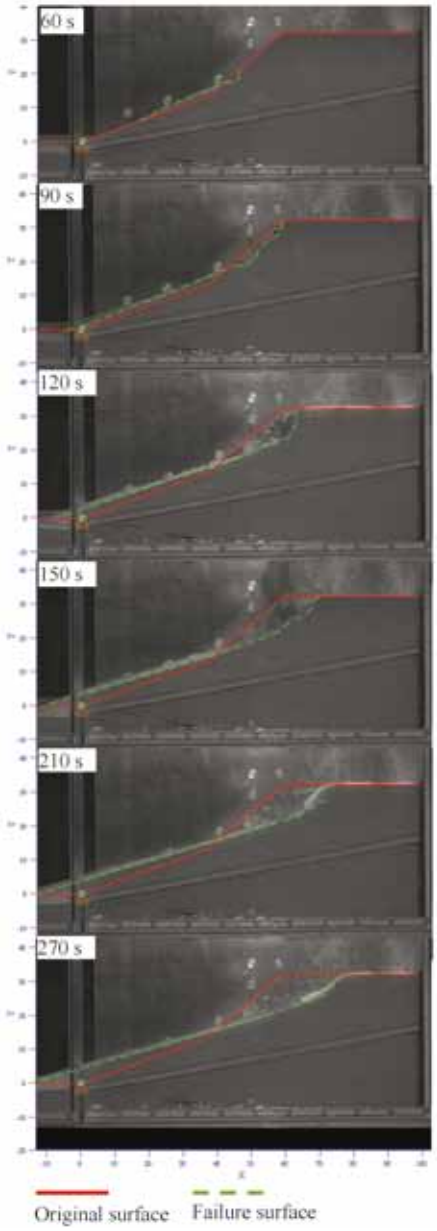

Fig. 2 - Failure surfaces for T2 at different times

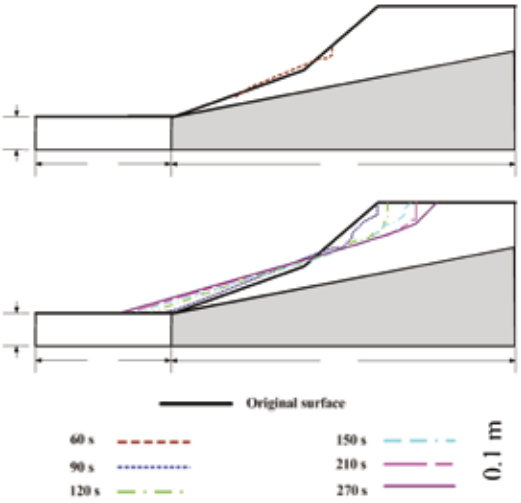

Fig. 3 - The retrogressive failure surfaces in a sandy soil slope (T2)

to induce piping at the toe of a slope. On the other hand, owing to water infiltrating more slowly in a silty sand, fines particles were washed out by water from the interstices at shallow depths and became fluidized. More details about each test are described as follows.

- Test T1 - As aforementioned, the wetting of slope started from the toe where piping occurred. This small zone of failure subsequently extended quickly upward to about the interface between lower and upper slopes, forming a shallow sliding. Later on the failure surface continued to deepen and extended beyond the crest to produce a deep failure. The extension of the collapsed area was about one half of the platform.
- Test T2 - The wetting of slope also began from the toe, in the same way as T1. However, due to an impervious dip stratum, initiation of piping and developing a shallow sliding were faster than T1 test. Even so the collapsed area on the platform was also about one half of the original area.
- Test T3 - In this test, the wetting of slope began from the interface between upper and lower slopes, but there was no obvious piping occurred in this silty sand as previously described. Instead, a crack on the platform was noticed first, which then developed quickly from a rill into a small gully. Figure 4 shows how the rill was eroded and turned into a gully. The final dimension of the eroded hole near the crest was about 0.13 m wide and 0.14 m deep.
- Test T4 - The applied rainfall intensity in this test was only one half of that in T3. Although initial failure starting from the toe of the slope was more obvious as compared to T3, it was less significant than T2. The failure mode tended to be a complex mode of flow and slide. An eroded gully was also developed on the surface of upper slope and extended upward to the crest. Nevertheless, this gully was only 0.067 m wide, about one half of that in T3.

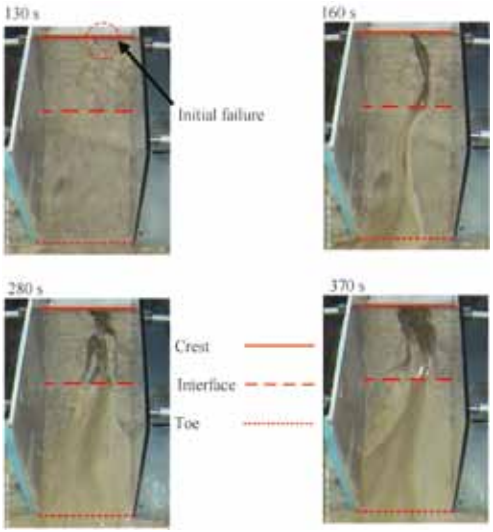

Fig. 4 - Top view of the failure process for T3

From Table 3 it can be seen that both t_p and t_f for T2 occurred sooner than T1; apparently, it was resulted from the dip stratum. With regard to samples A and B, both t_p and t_f of test T3 took place slower than test T2. The reason could be explained by the difference in the fines content and hydraulic conductivity of the sample. As to the effect of rainfall intensity on T3 and T4, it seems to be only more significant on t_p. Finally, the time to end mass movement, t_e, expectedly took longer for sample B than sample A.

VOLUMETRIC WATER CONTENT

The volumetric water content of soil was measured by seven sensors, and their coordinates with respect to the toe of the slope are given in Figure 1. The initial volumetric water content and the specific water contents corresponding to t_p, t_f, and t_e are denoted as θ_0, θ_p, θ_f, θ_e, respectively. These values are tabulated in Table 4.

Figure 5 shows the time histories of the volumetric water contents of W2 and W5; W2 was at the crest and W5 was at the interface of upper and lower slopes. It can be seen from Figure 5a that the curves of two samples display different trend, even though the initial values of the two samples were about the same. Since sample A is relatively permeable, hence the curves in Figure 5a1 did not reach full saturation. In addition to that, the curve of T2 declined significantly after tf, as opposed to that of T1. On the contrary, in Figure 5a2, the curves of sample B attained high values, and the curve of T3 could even reach complete saturation. Obviously, the phenomena were owing to the less permeable characteristic of sample B as well as the rainfall of higher intensity applied to T3.

Sensor	Test	θ_0 (%)	θ_p (%)	θ_f (%)	θ_e (%)
W1	T1	26.7	37.3	41.0	41.5
	T2	25.4	29.8	37.3	41.1
	T3	33.6	34.0	39.4	45.0
	T4	28.0	34.3	40.5	42.7
W2	T1	25.0	32.0	38.2	37.5
	T2	25.0	31.2	37.3	38.5
	T3	25.7	29.3	46.5	47.7
	T4	28.0	33.6	37.4	38.1
W5	T1	36.0	37.2	38.9	43.2
	T2	38.1	39.0	39.5	39.7
	T3	43.1	43.8	44.9	47.3
	T4	41.6	41.7	41.9	42.6
W7	T1	38.0	38.5	43.2	43.6
	T2	39.0	39.7	39.7	43.3
	T3	41.2	41.8	42.4	45.4
	T4	47.3	47.5	47.9	49.8

Tab. 4 - Summary of volumetric moisture contents

For W5 located at the interface of lower and upper slopes, all curves in Figures 5b had high initial values because the passage for flow became narrower adjacent to this area. In Figure 5b1, the curve of T2 was higher than that of T1, resulting from the narrow passage on the impervious stratum. In Figure 5b2, it is also not surprising to see the curve of T3 subjected to higher rainfall intensity was above that of T4. Another characteristic of the curves at this interface was none of them declined after t_f.

PORE-WATER PRESSURE

The variation of pore-water pressure in soil was recorded using six piezometers shown in Figures 1a and b. Piezometers P1 and P4 were below the right side of the platform, P2 and P5 were below the crest, and P3 and P6 were close to the toe of the slope. Their coordinates are given in Figure 1b. For convenience to compare, total head instead of piezometric head was adopted, taking the bottom of the model as the datum. The total head versus time are displayed in Figures 6a and b.

As illustrated in Figure 6a, the total head for sample A generally increased markedly from t_p to t_f. The period between t_p and t_f was shorter for T2 than that of T1, indicating failure occurred sooner in T2. After t_f, the total head either kept steady or even increased due to water was continuously supplied into the soil. On the other hand, the increase in total head from t_p to t_f for sample

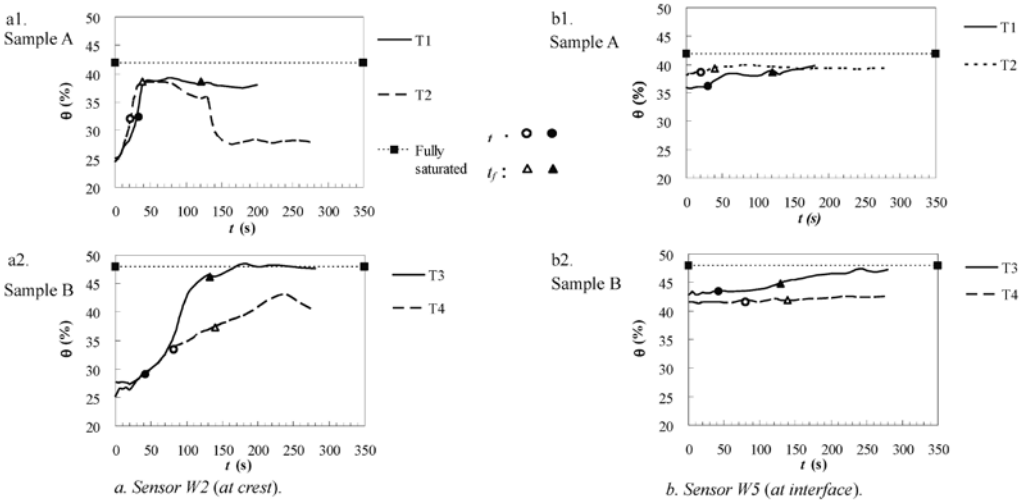

a. Sensor W2 (at crest). b. Sensor W5 (at interface).

Fig. 5 - Volumetric water content versus time obtained from moisture sensors W2 and W5

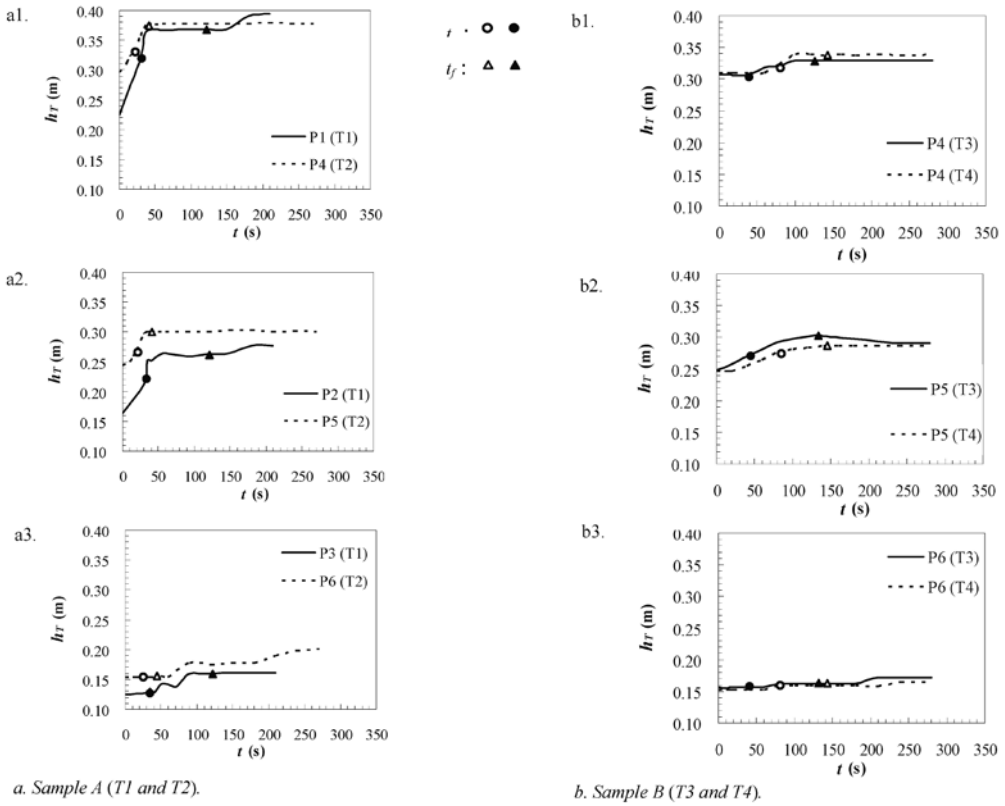

a. Sample A (T1 and T2). b. Sample B (T3 and T4).

Fig. 6 - Total head versus time for tests on different samples

B was less obvious. As can be seen from Figure 6b, t_f for both T3 and T4 were only slightly different; this has been indicated in Table 3. Furthermore, the total head after t_f essentially did not have a marked change. One exception, shown in Figure 6b2, is that a peak value was noticed at t_f. Apparently, this was related to the location of P5 from where the cross-sectional area gradually became smaller down to the toe of the slope, and

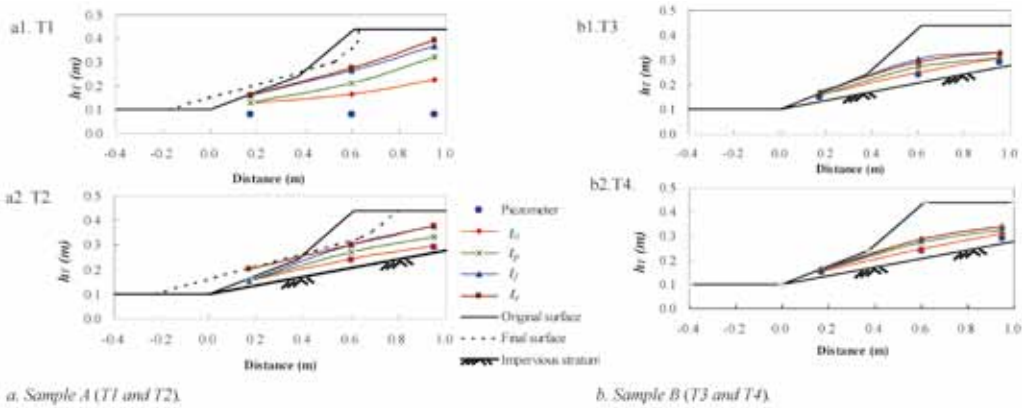

Fig. 7 - Profile of total head at different times in tests T1 ~ T4

therefore the pore-water pressure was easily to build up. Comparing respectively the dotted curves of P4, P5, and P6 in Figures 6a and b, the peak total heads in sample A were 0.05 ~ 0.08 m higher than those in sample B, as a result of more permeable nature of sample A.

In addition, the profiles of total head at different times for the four tests are illustrated in Figure 7. For homogeneous slope, T1, the profiles are concave, whereas those for T2-T4 are convex. Besides, the initial profiles of T2-T4 were approximately parallel to the impervious stratum. From this result, it is easy to know that the upper part of the slope was not saturated during the test. But most of the lower slope, especially near the toe, was saturated when slope failure occurred. As illustrated in Figure 7a2, the final total head at P6 approximated the final surface. This observation suggests a mode of retrogressive failure started from the toe of the slope.

The final surfaces of T1 and T2 are also plotted in Figures 7a1 and a2. Comparing these figures, T2 had a deeper failure and somewhat farther run-out distance. Nevertheless, the final surfaces for T3 and T4 are not plotted because there was no well defined failure surface observed.

CONCLUSIONS

This experiment employed rainfall induced overland flows to infiltrate into sandy soil slopes to study their stability. The characteristics of the failure mechanism and the responses of pore pressure and water contents in two samples composed of sand and silty sand, respectively, were observed.

The failure in permeable sand was a sliding mode. Initial failure was noticed as a piping occurred at the toe of slope, and it then gradually propagated upward as a retrogressive failure. Apart from this, the failure occurred in the slope with a dip stratum was fast (t_p = 20 s and t_f = 40 s), compared to that in the homogeneous slope (t_p = 30 s and t_f = 120 s). However, the failure in less permeable silty sand was initiated by erosion at shallow depth, the rill later expanded and turned into either a flow or a complex mode of flow and slide, depending on the rainfall intensity applied. Moreover, sandy soil had a marked increase in pore-water pressure when approaching failure; nevertheless, this phenomenon was less obvious for silty sand.

The initial profiles of total head in the slopes with a dip stratum were approximately parallel to the impervious stratum. Hence most of the lower slope, especially near the toe, was saturated when slope failure occurred. This observation also confirmed the observation that the mode of retrogressive failure started from the toe of sandy slopes.

The findings from this experiment are helpful to clarify the failure mechanisms of granular soil slopes such as the case study described in the introduction. It is also hoped that the observation from this experiment may provide a reference for numerical analyses as well as future remedial work for similar soil slopes.

ACKNOWLEDGEMENTS

This research was financially supported by the National Science Council, ROC.

REFERENCES

Brand E.W. (1982) - *Analysis and design in residual soil,* Proceedings of the ASCE Geotechnical Engineering Division, Specialty Conference- Engineering and Construction in Tropical and Residual Soils, Honolulu, Hawaii, 89-141.

Chen H., Chen R.H. & Lin M.L. (1999) - *Initiation of the Tungmen debris flow, eastern Taiwan*, Environmental and Engineering Geosciences, **5** (4): 459-473.

Chen H., Chen R.H., Yu F.C., Chen W.S. & Hung J.J. (2004) - *The Inspection of the triggering mechanism for a hazardous mudflow in an urbanized territory,* Environmental Geology, **45** (7): 899-906.

Chen R.H., Chen H.P. & Chen K.S. (2009) - *Simulation of a slope failure induced by rainfall infiltration,* Environmental Geology, **58** (5): 943-952.

Huang C.C., Lo C.L., Jang J.S. & Hwu L.K. (2008) - *Internal soil moisture response to rainfall-induced slope failures and debris discharge,* Engineering Geology, **101** (3): 134-145.

Iverson R.M. & Major J.J. (1986) - *Ground water seepage vectors and the potential for hillslope failure and debris flow mobilization*, Water Resources Research, **22** (11): 1543-1548.

Kim J., Jeong S., Park S. & Sharma J. (2004) - *Influence of rainfall-induced wetting on the stability of slopes in weathered soils*, Engineering Geology, **75** (3): 251-262.

Lumb P. (1975) - *Slope failure in Hong Kong*. Quarterly Journal of Engineering Geology, **8**: 31-65.

Moriwaki H., Inokuchi T., Hattanji T., Sassa K., Ochiai H. & Wang G. (2004) - *Failure processes in a full-scale landslide experiment using a rainfall simulator,* Landslides, **1** (4): 277-288.

Orense R.P., Shimoma S., Maeda K. & Towhata I. (2004) - *Instumented model slope failure due to water seepage*, Journal of Natural Disaster Science, **26** (1), 15-26.

Rocha M. (1957) - *The possibility of solving soil mechanics problems by the use of models* - 4th International Conference on Soil Mechanics and Foundation Engineering, London, U.K., **1**: 183-188.

Roscoe K. (1968) - *Soils and model tests* - Journal of Strain Analysis, **3**: 57-64.

Tohari A., Nishigaki M. & Komatsu M. (2007) - *Laboratory rainfall-induced slope failure with moisture content measurement,* Journal of Geotechnical and Geoenvironmental Engineering, **133** (5): 575-587.

Wang, G. & Sassa K. (2003) - *Pore-water pressure generation and movement of rainfall-induced landslides: effects of grain size and fine-particle content,* Engineering Geology, **69** (2): 109-205.

